Superstructure gratings in the tight-binding approximation

C. Martijn de Sterke*
School of Physics, Australia and Australian Photonics Cooperative Research Centre, University of Sydney 2006, Australian Technology Park, Eveleigh 1430, Australia
(Received 11 August 1997)

The reflection properties of gratings, such as those found in the core of an optical fiber, previously have been interpreted in terms of evanescent or propagating wave behavior in different parts of the grating. According to this interpretation, nonuniform gratings can thus be understood in a similar way to one-dimensional quantum-well structures. Here we exploit this similarity to develop an analytic theory for deep Bragg superstructure gratings. Using a method similar to the tight-binding method from condensed matter physics, we find approximate analytic expressions for the high- and low-reflectance frequency regions of such gratings. [S1063-651X(98)01003-4]

PACS number(s): 42.79.Dj, 42.81.Wg, 71.15.Fv

I. INTRODUCTION

Superstructure Bragg gratings (SSGs), or optical superlattices, are gratings with parameters that vary periodically as a function of position [1–7]. SSGs thus have two periodicities: one at the level of the wavelength of light, indicated by d, and a superstructure period Λ, which is typically 1 mm to 1 cm. To understand qualitatively the key properties of SSGs we consider the Fourier spectrum of the refractive index [2,3,7]. Since a uniform grating is characterized by a single period d, this spectrum consists of a series of frequency components, the lowest of which is at frequency $2\pi/d$. This leads to a reflection spectrum consisting of a peak at the Bragg frequency $f=c/2\overline{n}d$, where c is the speed of light in vacuum and $\overline{n}$ is the average refractive index in the grating; reflections associated with higher harmonics occur at much higher frequencies. In contrast, the spectrum of a SSG consists of contributions at frequencies $\ldots$, $2\pi(1/d-2/\Lambda)$, $2\pi(1/d-1/\Lambda)$, $2\pi/d$, $2\pi(1/d+1/\Lambda)$, $2\pi(1/d+2/\Lambda)$, $\ldots$, with the amplitudes of the various components depending on the details of the SSG. In the limit in which the SSG is weak, roughly corresponding to the condition that the SSG is a weak perturbation on a uniform grating, each Fourier coefficient of the refractive index distribution now leads to an associated peak in the reflection spectrum [2,3,7,8]. Thus the reflection spectrum of a SSG consists of peaks (Rowland ghosts [9]) at closely spaced frequencies clustered about the Bragg frequency [2,3]: $f_N=c/2\overline{n}(1/d+N/\Lambda)$, where $N=0,\pm1,\ldots$. Though this simple picture fails when the SSG is not shallow [7], it nevertheless gives an appealing intuitive understanding of the qualitative features of the reflection spectrum of a SSG.

The fact that the reflection spectrum of SSGs consist of lines that are approximately equally spaced has led to a number of applications, which have been realized in both semiconductor [2,6] and fiber geometries [3–5]. Applications include tunable distributed feedback lasers in semiconductors and fibers [2–4,6] and multichannel dispersion compensation in optical fibers [5]. SSGs also have interesting nonlinear optical properties [10,11], though we do not discuss these here.

Coupled-mode theory [8] is a widely used method to analyze gratings. In this method one works with the envelopes of electric field rather than with the field itself. This significantly reduces the complexity of the problem compared to solving Maxwell's equations directly. Nonetheless, in general one cannot find analytic expressions for key SSG parameters. An exception is shallow SSGs, to which the argument outlined in the first paragraph above can be applied. This Fourier argument does allow one, for example, to find analytic expressions for the widths of the highly reflective spectral regions. Here we develop the theory for the opposite limit, that of deep SSGs, for which analytic results can also be obtained.

To find analytic results for deep SSGs it is important to note that coupled-mode theory allows one to understand SSGs in a way complementary to the Fourier argument described in the first paragraph above (though the Fourier argument also follows from coupled-mode theory). According to coupled-mode theory, the field envelope in a uniform grating is evanescent for frequencies close to f_B, leading to strong reflection, whereas it is propagating sufficiently far from f_B [12]. Thus, for frequencies sufficiently close to f_B the grating acts as if it were a potential barrier. A SSG, in which the grating parameters vary periodically, can be thought of as a periodic array of potential barriers, separated by potential wells [12]. From the physics of crystalline solids we know that such periodic arrays lead to bands, separated by gaps [13]. A SSG can be understood similarly: The periodicity gives rise to (photonic) bands where the reflectivity is low, separated by (Rowland ghost) gaps, where the reflectivity is high. Here we make use of this interpretation of SSGs in terms of wells and barriers. In particular, we adapt the tight-binding method [13], developed to determine the properties of crystalline solids, to SSGs and use it to find approximate analytic expressions for the high- and low-reflectivity spectral regions, as well as analytic expressions for the associated eigenfields. It should be noted that although these results are important in their own right, they are also the start-

*FAX: (612) 9351 7726. Electronic address: desterkephysics.usyd.edu.au

ing point for quantitative analyses of SSGs, in both linear and nonlinear regimes [7].

In Sec. II we review coupled-mode theory and introduce the concept of well and barrier in this context. In Sec. III we consider a general photonic well and find the transcendental equation determining its bound states. Then in Sec. IV we study three simple well types in some detail. In Sec. V we use some of these results, in combination with the tight-binding method, to find the photonic bands of deep SSGs. A discussion and conclusions follow in Sec. VI.

II. COUPLED-MODE THEORY AND SUPER-COUPLED-MODE THEORY

As mentioned, coupled-mode theory [8] is widely used to calculate the properties of gratings. In its standard form it can be used whenever the grating is shallow and it can thus be applied to all fiber gratings and to most gratings in semiconductors [14]. The key feature of coupled-mode theory is that one uses electric-field envelopes rather than the electric field itself. When applied to a uniform grating one can then replace the wave equation with a periodic refractive index, with a set of coupled-mode equations with constant coefficient [8,12]. To accomplish this we write the refractive index n as

$$n(x)=n_0+\delta n(x)+\Delta n(x)\cos\left(\frac{2\pi x}{d}+\vartheta(x)\right), \tag{1}$$

where $\delta n(x)$, $\Delta n(x)$, and $\vartheta(x)$ define the superstructure and are periodic functions of position. Here n_0 is a reference refractive index, δn is a small deviation of the average refractive index from n_0, Δn is the grating strength, d is the nominal grating period, and $\vartheta(x)$ represents periodic variations of the period. The electric field E is written as

$$E(x,t)=[E_+(x,t)e^{+i(k_0x+\vartheta/2)} +E_-(x,t)e^{-i(k_0x+\vartheta/2)}]e^{-i\omega_0t}+\text{c.c.}, \tag{2}$$

where $E_\pm$ are the envelopes of the forward and backward propagating modes, $k_0=\pi/d$, and ω_0 is the associated (Bragg) frequency. It can then be shown that the $E_\pm$ satisfy the coupled-mode equations [8,12]

$$+i\frac{\partial E_+}{\partial x}+\frac{i}{v_g}\frac{\partial E_+}{\partial t}+\kappa(x)\,E_-+\delta(x)\,E_+=0,$$
$$-i\frac{\partial E_-}{\partial x}+\frac{i}{v_g}\frac{\partial E_-}{\partial t}+\kappa(x)\,E_++\delta(x)\,E_-=0, \tag{3}$$

where v_g is the group velocity at ω_0 in the absence of the grating and κ and δ are given by

$$\kappa(x)=\frac{\pi\Delta n(x)}{\lambda},$$
$$\delta(x)=\frac{2\pi\delta n(x)}{\lambda}-\frac{1}{2}\frac{d\vartheta}{dx} \tag{4}$$

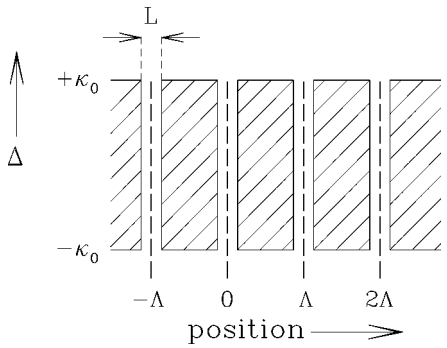

FIG. 1. Band diagram of the SSG defined by Eq. (8) and $\delta=0$. Dashed regions indicate values of the detuning for which, as a function of position, the field envelopes are evanescent, while in the clear regions they are propagating.

and thus characterize the grating. For a uniform grating δ and κ are constants, whereas for a SSG they are periodic functions.

We now first consider uniform gratings for which δ and κ are constants [8]. Assuming a harmonic time dependence, so that

$$E_\pm(x,t)=e^{-iv_g\Delta t}F_\pm(x), \tag{5}$$

where Δ is the detuning, we find that the envelopes $F_\pm$ satisfy

$$+i\frac{\partial F_+}{\partial x}+\kappa(x)\,F_-+[\delta(x)+\Delta]\,F_+=0,$$
$$-i\frac{\partial F_-}{\partial x}+\kappa(x)\,F_++[\delta(x)+\Delta]\,F_-=0. \tag{6}$$

From these it is easy to see that if

$$-\delta-\kappa<\Delta<-\delta+\kappa, \tag{7}$$

the envelope is evanescent, whereas otherwise it is propagating [12]. As mentioned, this result is related to the high grating reflectivity for frequencies around the Bragg frequency.

To understand how we analyze SSGs we consider as an example the simple case where $\delta n=0$, $\vartheta=0$, so that by the second of Eqs. (4) $\delta=0$ as well. Further,

$$\kappa=\begin{cases}0 & \text{if } M\Lambda-\dfrac{L}{2}<x\leqslant M\Lambda+\dfrac{L}{2}\\[2ex] \kappa_0 & \text{if } M\Lambda+\dfrac{L}{2}<x\leqslant(M+1)\Lambda-\dfrac{L}{2}\end{cases}, \tag{8}$$

where $M=0,\pm1,\pm2\ldots$. This is thus a SSG in which the grating periodically vanishes. Here Λ is the SSG's period, and L is the width of the ''empty'' regions. Figure 1 is the band diagram [12,15] of the SSGs defined by Eq. (8): The dashed regions in Fig. 1 show the values of the detuning Δ for which, as a function of position, the field envelopes are evanescent according to Eqs. (8) and (7), whereas in the clear regions the envelope is propagating.

Since SSGs, such as that in Fig. 1 thus correspond to a periodic array of regions with evanescent and propagating wave behavior, they can be interpreted as a periodic array of wells (clear regions in Fig. 1), and barriers (dashed regions). SSGs are thus similar to the Schrödinger equation with one-dimensional periodic potentials [16]. It is one of the aims here to exploit this similarity.

It is well known that solutions to the Schrödinger equation with periodic potential can be obtained numerically or sometimes from a simple transcendental equation in the case of the Kronig-Penney model; these solutions entail the electronic band structure and the associated Bloch functions [13]. Analytic results can be obtained in limiting cases. For example, when the periodic component of the potential is weak, the *nearly free electron approximation* applies [13]. In the opposite limit, regions of low potential are considered to be wells, separated by potential barriers. The *tight-binding approximation* can be used if the interaction between the eigenfields in different wells is small, which occurs when the barriers are sufficiently strong [13]. It was shown earlier that the numerical method [7] and the nearly free electron method [2,3,7] used in solid state physics adapt straightforwardly to the case of SSGs [7]. Here we adapt the tight-binding method to SSGs and use it to find approximate analytic expressions for the (photonic) bands and for the Bloch functions for deep SSGs [7].

Analytic expressions for the photonic bands and the Rowland ghost gaps indicate for which values of the detuning [Eq. (5)] the SSG is reflecting, but the actual level of reflectance cannot be determined in this way. However, it has been shown that the additional information contained in the Bloch functions can be used to estimate the reflectivity as a function of detuning [7].

III. PHOTONIC WELLS

Here we derive expressions that determine the positions of the discrete levels of a single photonic well. We do so for the general type with piecewise constant parameters, as illustrated in the band diagram [12,15] shown in Fig. 2. The subscripts W refer to well parameters, whereas B refers to barrier parameters. For this structure to act as a potential well with discrete bound states, the envelopes must be propagating for $|x|<L/2$ and evanescent for $|x|>L/2$. From Fig. 2 we see that we thus only consider detunings Δ such that

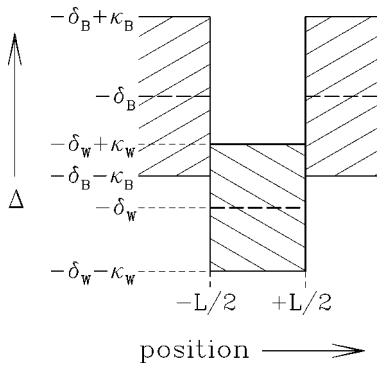

FIG. 2. Band diagram for a general photonic well. The subscripts B refer to barrier parameters, while W refers to the well. The dashed regions indicate evanescent behavior of the field envelopes and the clear regions indicate propagating behavior.

$$-\delta_W+\kappa_W<\Delta<-\delta_B+\kappa_B. \tag{9}$$

A discrete level of the potential well in Fig. 2 must be a solution to the coupled-mode equations (6) in which the envelopes $E_\pm$ vanish as $x\to\pm\infty$. To find such solutions we first use the transfer matrix of Eqs. (6) if κ and δ are constants [7]. It is easy to see that

$$\begin{pmatrix} F_+(x) \\ F_-(x) \end{pmatrix} = M \begin{pmatrix} F_+(0) \\ F_-(0) \end{pmatrix}, \tag{10}$$

where the transfer matrix M is given by

$$M=\begin{pmatrix} \cosh\alpha x+i\dfrac{\delta+\Delta}{\alpha}\sinh\alpha x & i\dfrac{\kappa}{\alpha}\sinh\alpha x \\ -i\dfrac{\kappa}{\alpha}\sinh\alpha x & \cosh\alpha x-i\dfrac{\delta+\Delta}{\alpha}\sinh\alpha x \end{pmatrix}, \tag{11}$$

where

$$\alpha=\sqrt{\kappa^2-(\delta+\Delta)^2}. \tag{12}$$

In a discrete level there is no net energy transfer and so the eigenfield must have the property

$$|F_+|^2=|F_-|^2; \tag{13}$$

we note that this is equivalent to the quantum-mechanical property that the wave function associated with a bound state can be made real [16]. Using transfer matrix (11), it is easy to see that for the envelopes to vanish as $x\to+\infty$, at $x=L/2$, envelopes $F_\pm$ must be related by

$$\begin{pmatrix} F_+(L/2) \\ F_-(L/2) \end{pmatrix} = F_{+R} \begin{pmatrix} 1 \\ e^{i\varphi_R} \end{pmatrix}, \tag{14}$$

where F_{+R} is a normalization constant and

$$e^{i\varphi_R}=\frac{-\delta_B+i\alpha_B}{\kappa_B}. \tag{15}$$

Note that Eq. (14) satisfies condition (13). One can define F_{+L} and φ_L at $x=-L/2$ similar to Eqs. (14) and (15). Now using transfer matrix (11) in the well, one can relate the envelopes at $x=\pm L/2$, leading to a set of transcendental equations. The result is

$$\cos(\alpha_W L)+\frac{\alpha_B}{\kappa_B}\frac{\kappa_W}{\alpha_W}\sin(\alpha_W L)=\mp\frac{\delta_B+\Delta}{\kappa_B},$$
$$\left(\frac{\delta_W+\Delta}{\alpha_W}-\frac{\delta_B+\Delta}{\kappa_B}\frac{\kappa_W}{\alpha_W}\right)\sin(\alpha_W L)=\mp\frac{\alpha_B}{\kappa_B}, \tag{16}$$

both of which must be satisfied simultaneously. We note that Eqs. (16) are consistent in that simultaneous solutions can always be found. Note also that Eqs. (16) are of the same general type as the transcendental equations for the level of a well in quantum mechanics [16].

Since the envelopes can be multiplied by an arbitrary constant phase, we choose the constant F_{+R} in definition (14) to be real (its magnitude is determined by normalization). Then, if the upper (lower) of the two signs applies, at $x=-L/2$,

$$\begin{pmatrix}F_+(-L/2)\\F_-(-L/2)\end{pmatrix}=\pm F_{+R}\begin{pmatrix}e^{i\varphi_R}\\1\end{pmatrix}, \tag{17}$$

where both signs are allowed.

In Sec. IV we seek solutions to Eqs. (16) and the associated eigenfunctions for three types of wells.

IV. EIGENSTATES AND EIGENFIELDS OF PHOTONIC WELLS

We now consider solutions to transcendental equations (16) for three special cases. In the first, to be discussed in Sec. IV A, we take $\kappa_W=0$ and $\delta_W=\delta_B$, leading to the situation as in Fig. 1; we refer to this as an *unshifted empty well*. The second type, the *shifted empty well*, is similar to the previous type in that $\kappa_W=0$, but is more general since δ_W and δ_B are arbitrary. It is discussed in Sec. IV B. The third special case, discussed in Sec. IV C, is that in which $\kappa_B=\kappa_W$ and $\delta_B\neq\delta_W$ (see Fig. 2); this type is referred to as having an *equal well and barrier*. The unshifted empty well is treated in the most detail, as only this type is used to construct tight-binding solutions for SSGs in Sec. V.

A. Unshifted empty wells

Here we consider the eigenvalues and eigensolutions for wells for which $\kappa_B=\kappa_0$, $\kappa_W=0$, and $\delta_B=\delta_W=0$; note that the last of these equalities does not imply any loss of generality, as it simply fixes the frequency for which $\Delta=0$. Equation (16) now reduce to

$$\cos(\Delta L)=\mp\frac{\Delta}{\kappa_0},$$
$$\sin(\Delta L)=\mp\frac{\sqrt{\kappa_0^2-\Delta^2}}{\kappa}. \tag{18}$$

Note that the number of solutions of Eqs. (18) is always even, since if Δ is a solution with the top sign applying, then $-\Delta$ is a solution with the bottom sign. Further, the number of solutions increases with $\kappa_0 L$; this is expected as $\kappa_0 L$ represents the well's strength. The number of solutions can be found to be the smallest integer larger than or equal to $\kappa_0 L/\pi$. Hence, as $\kappa_0 L\to 0$, there are two solutions, which are increasingly poorly bound. Of course this behavior is similar to that of one-dimensional quantum wells, which always support at least a single state. In analogy, we refer to the states that remain bound as $\kappa_0 L\to 0$ as the well's ground states.

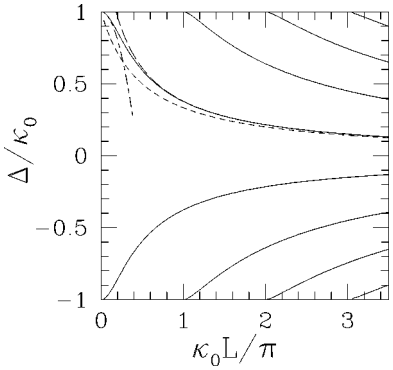

FIG. 3. Eigendetunings Δ of the eigenstates for a well with $\kappa_W=0$ and $\delta_W=\delta_B=0$, as a function of the well strength $\kappa_0 L$ (solid lines). The short- and long-dashed lines are lower and upper limits, respectively, given in inequality (20); the long-dash–short-dashed line indicates an approximative result discussed in the text.

The solid lines in Fig. 3 show the positions of the various eigenstates as a function of the well strength $\kappa_0 L$. It is consistent with the properties discussed above. The long-dash–short-dashed line is given by $\Delta/\kappa_0=1-(\kappa_0 L)^2/2$, which is the lowest-order approximate solution as $\kappa_0 L\to 0$ for the ground-state solution with $\Delta>0$. Additional approximations can be obtained from the inequality

$$1-\frac{2}{\pi}x\leqslant\cos x\leqslant\frac{\pi}{2}-x \tag{19}$$

for $|x|\leqslant\pi/2$. With a straightforward generalization to other arguments, we find from Eqs. (18) and (19) that

$$\frac{2N+1}{1+2\kappa_0 L/\pi}\leqslant\frac{\Delta}{\kappa_0}\leqslant(2N+1)\frac{\pi/2}{\kappa_0 L+1}, \tag{20}$$

where $N=0,\pm 1,\pm 2,\ldots$. The short- and long-dashed curves indicate, respectively, these lower and upper bounds for the upper of the two ground states in Fig. 3; clearly the convergence is excellent, especially for $\kappa_0 L\gtrsim\pi$.

By direct calculation it can be shown that the eigenfunctions, indicated by Ψ_W, are given by

$$\Psi_W=\mp C\begin{pmatrix}e^{i\varphi_R}\\1\end{pmatrix}e^{+\alpha(x+L/2)},\quad x<-\frac{L}{2}$$
$$\Psi_W=\mp C\begin{pmatrix}e^{i\varphi_R}e^{i\Delta(x+L/2)}\\e^{-i\Delta(x+L/2)}\end{pmatrix},\quad -\frac{L}{2}\leqslant x\leqslant\frac{L}{2} \tag{21}$$
$$\Psi_W=C\begin{pmatrix}1\\e^{i\varphi_R}\end{pmatrix}e^{-\alpha(x-L/2)},\quad x>\frac{L}{2},$$

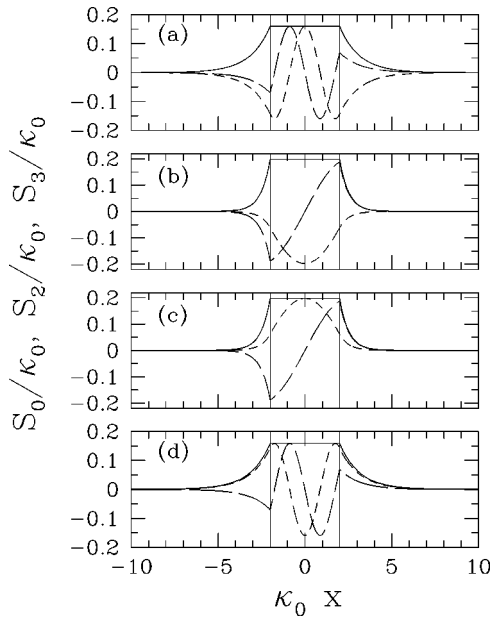

FIG. 4. Eigenfields of the four bound states of a well with $\kappa_0 L=4$. Results are shown for (a) $\Delta=0.8988$, (b) $\Delta=0.3131$, (c) $\Delta=-0.3131$, and (d) $\Delta=-0.8988$. Indicated are $S_0=|\psi_+|^2+|\psi_-|^2$ (solid lines), $S_2=\psi_+\psi_-^*+\psi_-\psi_+^*$ (short-dashed lines), and $S_3=i(\psi_+\psi_-^*-\psi_-\psi_+^*)$ (long-dashed lines). The vertical lines indicate the well edges. By showing S_i/κ_0 versus $\kappa_0 x$ the result does not depend on κ_0.

where the signs correspond to those in Eqs. (16). Further, the constant

$$C=\sqrt{\frac{\alpha}{2(\alpha L+1)}} \tag{22}$$

is determined by the normalization $\int_{-\infty}^{\infty}\Psi^\dagger\Psi dx=1$ [7] and φ_R was defined in Eq. (15). By direct calculation it can be confirmed that the various eigenfunctions are mutually orthogonal.

Figure 4 shows the eigenfunctions for an empty unshifted well as a function of position. We take $\kappa_0 L=4$, so that, according to our earlier argument, the well has four discrete eigenstates. Figure 4(a) shows the result for $\Delta=0.8988$, Fig. 4(b) for $\Delta=0.3131$, Fig. 4(c) for $\Delta=-0.3131$, and Fig. 4(d) for $\Delta=-0.8988$. The various line types indicate three of the Stokes parameters [17] that can be constructed from the eigenfields. Indicating the components of Ψ by $\psi_\pm$, these can be written as $S_0=|\psi_+|^2+|\psi_-|^2$ (solid lines), $S_2=\psi_+\psi_-^*+\psi_-\psi_+^*$ (short-dashed lines), and $S_3=i(\psi_+\psi_-^*-\psi_-\psi_+^*)$ (long-dashed lines). Recall that according to Eq. (13) the fourth Stokes parameter $S_1=|\psi_+|^2-|\psi_-|^2=0$. Note that by showing S_i/κ_0 versus $\kappa_0 x$ in Fig. 4, the results do not depend on the value of κ_0.

Many of the features in Fig. 4 are easily understood. For example, S_0 is constant in the well region because $\kappa_W=0$. Further, from Eq. (21) it can also be seen that S_0 and S_2 are even under changing the sign of x, whereas S_3 is odd. Next, for the two fundamental states at $\Delta=\pm 0.3131$, S_2 has no nodes, whereas for the next higher states at $\Delta=\pm 0.8988$, S_2 has a two nodes, similarly to the properties of quantum wells according to the one-dimensional Schrödinger equation [16].

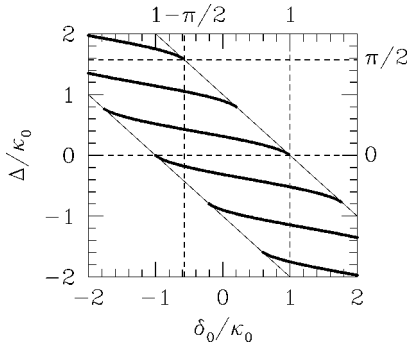

FIG. 5. Positions of the discrete eigenstates of a shifted empty well with $\kappa_0 L=4$. Shown is the eigendetuning Δ vs the barrier shift δ_0, both normalized with respect to κ_0. As discussed in the text, all solutions must lie between the two diagonal lines. The horizontal and vertical dashed lines follow from Eqs. (25).

Note finally that although the fields and the various Stokes parameters are continuous, the derivatives are not. The exception is S_2, but this is a particular property of the simple well considered here in which $\delta(x)$ is constant.

B. Shifted empty wells

Here we again consider the eigenvalues and eigensolutions for wells for which $\kappa_W=0$, but unlike the wells in Sec. IV A, now $\delta_W\neq\delta_B$. Then Eqs. (16) reduce to

$$\cos(\Delta L)=\mp\frac{\delta_0+\Delta}{\kappa_0},$$
$$\sin(\Delta L)=\mp\frac{\alpha_0}{\kappa_0}, \tag{23}$$

where, without loss of generality, we have taken $\delta_W=0$ and we have set $\delta_B=\delta_0$, and similarly for κ and α.

Since we are interested in bound states only, the solutions of interest have detunings such that

$$-\delta_0-\kappa_0\leqslant\Delta\leqslant-\delta_0+\kappa_0, \tag{24}$$

following the same argument as that leading to Eq. (9). In Fig. 5, which shows the positions of the eigenstates as a function of δ_0 for a well with $\kappa_0 L=4$, inequalities (24) indicate the diagonal lines. Note that for $\delta_0=0$ in Fig. 5, the same situation as in Sec. IV A ensues.

Figure 5 shows that the positions of the bound states with respect to extremes (24) vary as a function of δ_0 and that for certain values of δ_0 a bound state merges with the continuum. Hence the number of bound states depends on δ_0. For example, whereas for $\delta_0=0$ there are four bound states, for $\delta_0=0.4$ there are only three. It is easy to show that for a given value of $\kappa_0 L$ states merge with the continuum when

$$\frac{\delta_0}{\kappa_0}=\pm 1+\frac{N\pi}{\kappa_0 L},\quad \frac{\Delta}{\kappa_0}=-\frac{N\pi}{\kappa_0 L}, \tag{25}$$

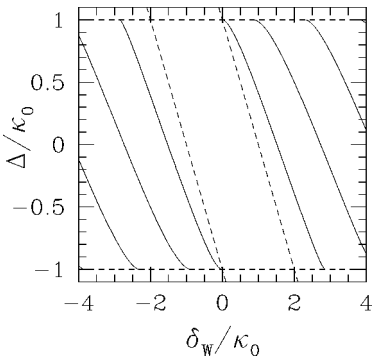

FIG. 6. Positions of the discrete eigenstates for a structure with $\delta_B=0$ and $\kappa_B=\kappa_W\equiv\kappa_0$ (solid lines) vs δ_W/κ_0. The dashed lines indicate the boundaries of regions for which no such states can exist.

where the upper (lower) sign refers to the upper (lower) diagonal line. A few of these (with the upper signs applying and $N=-2$ and 0) are indicated by the horizontal and vertical dashed lines in Fig. 5.

The eigenfields associated with the states of a shifted, empty well are similar to those in Fig. 4. The main difference is that dS_2/dx is not continuous as in Fig. 4 because δ is discontinuous. Apart from this the number of nodes, discussed at the end of Sec. IV A, is unchanged. This implies, in particular, that if δ_0 is sufficiently large ($\delta_0>1+\pi/4$ in Fig. 5), then the well does not support a ground state for which S_2 has no nodes (see Fig. 4).

C. Equal wells and barriers

Here we consider wells for which $\kappa_W=\kappa_B\equiv\kappa_0$ and $\delta_W\neq\delta_B$. Without loss of generality we set $\delta_B=0$. Dispersion relations (16) then reduce to

$$\cos(\alpha_W L)+\frac{\alpha_B}{\alpha_W}\sin(\alpha_W L)=\mp\frac{\Delta}{\kappa_0},$$
$$\frac{\delta_W}{\alpha_W}\sin(\alpha_W L)=\pm\frac{\alpha_B}{\kappa_0}. \tag{26}$$

Solutions to Eqs. (26) are shown in Fig. 6 for a well with $\kappa_0 L=2$. The solid lines show the eigendetuning Δ vs well shift δ_W, both normalized with respect to κ_0. Note that for $\delta_W=0$, corresponding to a uniform grating, the structure supports no bound states, as required. However, for finite δ_W at least a single such state can be found. The dashed lines in Fig. 6 bound the regions for which bound states can exist. The horizontal dashed lines indicate that for detunings such that $|\delta|>\kappa_0$ the field is not evanescent as $|x|\to\infty$, whereas between the diagonal dashed lines, given by $\Delta/\kappa_0=\delta_W/\kappa_0\pm1$, no bound states exist because the envelope is evanescent everywhere.

From Eqs. (26) it can also be derived that discrete eigenstates merge with the continuum when

$$\frac{\delta_W}{\kappa_0}=\pm\left[1\pm\sqrt{1+\left(\frac{\pi N}{\kappa_0 L}\right)^2}\ \right], \tag{27}$$

where the signs are unrelated, and $N=\pm1,\pm2,\ldots$. The eigenfields are again similar to those in Fig. 4, but with two key differences. First, since here $\kappa_W\neq0$, S_0 in the well is not constant. Second, since κ is constant, whereas δ is not, the Stokes parameter S_3 has a continuous first derivative, whereas that of S_2 is discontinuous at the interfaces, as can be seen directly from Eqs. (3).

V. TIGHT-BINDING APPROACH TO SSGS

Here we apply the tight-binding approach [13] to find approximations to the properties of SSGs, based upon the results for a single well. As in the theory for the Schrödinger equation with a periodic potential, we expect in a SSG the eigenstates of individual wells to broaden, to form bands [13]. These bands are separated by (Rowland ghost) gaps, where the transmittance is small.

Though the initial derivation is general, it is applied to the SSG given by Eq. (8) and $\delta=0$, with the band diagram shown in Fig. 1. In the tight-binding approach, such an SSG is considered to consist of a periodic array of unshifted empty wells as discussed in Sec. IV A.

In deriving the tight-binding results we closely follow the derivation of Chap. 9 in the text by Ashcroft and Mermin [13]. We write Eqs. (6) for a SSG as

$$M\mathbf{F}\equiv(M_W+\Delta M)\mathbf{F}=\Delta(k)\mathbf{F}, \tag{28}$$

where $\mathbf{F}$ indicates the column vector with components $F_\pm$ and operator M follows directly from Eqs. (6); in this problem it plays a similar role to the potential in the Schrödinger equation. Since M represents a SSG, it must be periodic (with period Λ). In the spirit of the tight-binding method we write this operator as the sum of M_W, the operator associated with a single well, such as those studied in Sec. IV, and $\Delta M\equiv M-M_W$. The eigenfields Ψ_W of M_W, which, in principle, can be calculated straightforwardly (see Sec. IV), satisfy

$$M_W\Psi_W=\Delta_W\Psi_W. \tag{29}$$

For an unshifted empty well, Ψ_W is given by Eqs. (21), whereas Δ_W follow from Eqs. (18). Finally, the right-hand side of Eq. (28) explicitly indicates that in periodic structures the eigendetunings are a function of the reduced wave number k [13]. In the subsequent analysis $M-M_W$ is considered small, so that it can be treated perturbatively.

In the tight-binding scheme the eigenfield for a SSG, in its most general form, is written as a superposition of the eigenfields of the individual wells as [13]

$$\mathbf{F}=\sum_N\sum_j b_j e^{ikN\Lambda}\ \Psi_{W,j}(x-N\Lambda), \tag{30}$$

where the b_j are constant coefficients. Here the summation over N includes all the wells in the SSG and the summation over j includes all bound states of each well.

In the calculation below we find that all contributions to the expressions for the features of the photonic bands and the associated eigenfields contain some positive integer power of the parameter $\epsilon\equiv\exp(-\alpha\Lambda)$ roughly corresponding to the decay of the envelope function in the barrier region between

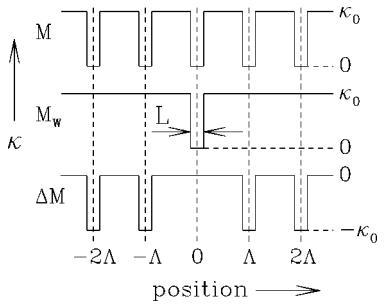

FIG. 7. Schematic of the generalized potentials M, M_W, and ΔM for an unshifted empty well.

two wells [cf. Eq. (21)]. Because of the assumption that the tight-binding approach applies, the barriers can be taken to be sufficiently thick so that $\epsilon \ll 1$. Here we are interested in the lowest-order results and we thus ignore all second- and higher-order contributions in ϵ.

Within the limitation described in the paragraph above, the summation over j in ansatz (30) can be dropped. This is so since for a particular well state, the effects of other states are ignored, as they affect the results only to second and higher orders in ϵ. Now by substituting ansatz (30) into Eq. (28) and following the procedure described by Ashcroft and Mermin, which makes use of Eq. (29), it is found that

$$\Delta(k) = \Delta_W + 2\cos(k\Lambda) \int_{\Lambda - L/2}^{\Lambda + L/2} \Psi^\dagger(x)\ \Delta M\ \Psi(x-\Lambda)\ dx \tag{31}$$

to first order in ϵ. Note that since the average of the cosine in result (31) vanishes, to this order the photonic band forms symmetrically about the eigendetuning of the bound state of the isolated well.

To evaluate the integral in Eq. (31), recall that according to Eq. (28) operator ΔM represents the difference between the SSG ''potential'' M and the well ''potential'' M_W. This is illustrated in Fig. 7, which shows schematically the parameter κ associated with M, M_W, and ΔM for an SSG given by Eq. (8) and $\delta = 0$.

Equation (31) can now be evaluated by substituting expression (21) for the eigenfield and using the definition of ΔM, illustrated in Fig. 7. Note that the integration can be limited to nearest-neighbor wells, as only these lead to contributions linear in ϵ. This leads to

$$\int_{\Lambda - L/2}^{\Lambda + L/2} \Psi^\dagger(x) \Delta M \Psi(x-\Lambda) dx = \pm \frac{\alpha}{\alpha L + 1} \frac{\alpha}{\kappa} e^{-\alpha(\Lambda - L)}, \tag{32}$$

which clearly is of first order in ϵ. We note that the choice of signs in Eq. (32) is the same as in Eqs. (21).

Figure 8 can be used to judge the accuracy of approximations (31) and (32). Shown are the positions of the lower and upper edges of the upper ground state of the empty, unshifted SSG with $\kappa_0 L = 1$, for various different values for $\kappa_0 \Lambda$ (see also Fig. 1). In particular, shown are the positions of the lower and upper edges of the upper ground state of the empty, unshifted SSG, according to the tight-binding analysis (solid lines) and according to exact numerical calculations (dots). Clearly, with decreasing Λ the wells are increasingly strongly coupled and the level becomes bandlike; according to Eq. (32), the tight-binding analysis predicts that the bandwidth scales with $\exp(-\alpha\Lambda)$.

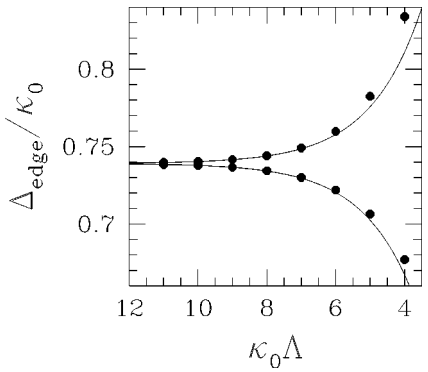

FIG. 8. Position of the top and bottom edges of the photonic band associated with the upper ground state of an empty, unshifted SSG with $\kappa_0 L = 1$, as a function of $\kappa_0 \Lambda$. The solid lines indicate the tight-binding results using Eqs. (31) and (32), whereas the dots represent exact numerical results.

Clearly, the tight-binding results are accurate if $\kappa_0 \Lambda \gtrsim 5$, but they are unsatisfactory for smaller $\kappa_0 \Lambda$. Note that the most obvious deviation of the tight-binding result is a shift of the average value of the edges, corresponding to a rigid shift of the band. Such a shift does come out of the tight-binding analysis, but to order ϵ^2.

Results such as those in Fig. 8 let one make some predictions about the SSG's reflection spectrum: Within the photonic band the envelope has propagating behavior and the SSG's reflectance is small. In contrast, in a Rowland ghost gap the envelope is evanescent and the reflectance approaches unity if the SSG is sufficiently long.

VI. DISCUSSION AND CONCLUSIONS

The results from Sec. V allow us to draw some important conclusions about Rowland ghost gaps and their spacing (in detuning). Let us first consider the spacing between adjacent Rowland ghost gaps. According to inequality (20), the levels of an unshifted, empty well are roughly equally spaced at a detuning of π/L if $\kappa_0 L \gg 1$. Whereas an equal spacing is also found for shallow SSGs (see the discussion in Sec. I), the quantitative differences are notable: in shallow SSGs, adjacent Rowland ghost gaps are spaced by π/Λ. However, in the tight-binding result it depends on the well width, whereas for shallow SSGs it depends on the SSG period.

It should also be noted that it is, in principle, straightforward to extend the present analysis to include higher-order terms in ϵ. In particular, one can identify a number of different contributions at order ϵ^2. These include a contribution in $\cos(k\Lambda)$ as in Eq. (31), as well as a dc shift of the band, and a contribution at $\cos(2k\Lambda)$ that leads to a change in the band's shape. In addition, there is also a contribution due to the presence of other levels in the isolated well. This leads to a set of simultaneous equations rather than to the single equation (31).

In conclusion, we have developed a tight-binding approach to describe the properties of deep SSGs. This allows us to find approximate analytic expressions for the highly reflecting spectral regions of the grating. Although in the

general case analytic expressions cannot be found, the Fourier-based theory [2] and the theory developed here can give some insight as they are applicable in the two extreme limits in which the superstructures are shallow and deep, respectively.

In using the tight-binding approach the bands and gaps of a SSG are considered to be associated with levels of single, isolated wells. When the wells are sufficiently close together, these levels broaden to give rise to bands (see Fig. 8). An intrinsic limitation of the tight-binding method can be seen from inequality (9), which gives the detunings for which the outer gratings act as barriers. Only detunings satisfying this inequality can be considered, even though it is known that Rowland ghost gaps occur at other values of the detuning as well. These have to be described using other methods. Nonetheless, the detunings for which the tight-binding method can be used generally exhibit the strongest reflections.

From Fig. 8 it is clear that for detunings that satisfy inequality (9), the tight-binding method gives satisfactory results if the bands are sufficiently narrow. The analysis also allows us immediately to draw conclusions about the reflectivity of the SSG, though at the level considered here these are only qualitative. Nonetheless, the photonic band structure and the associated eigenfields can be used as inputs in supercoupled-mode theory. This theory lets one find the SSG reflectivity and can also include, if required, nonlinear effects [7]. This will be the subject of a future work.

ACKNOWLEDGMENTS

I am grateful to Neil Broderick and Ben Eggleton for many discussions on SSGs. This work was supported by the Australian Research Council.

[1] P. St. J. Russell, J. Appl. Phys. **59**, 3344 (1986).
[2] V. Jayaraman, Z.-M. V. Chuang, and L. A. Coldren, IEEE J. Quantum Electron. **29**, 1824 (1992).
[3] B. J. Eggleton, P. A. Krug, L. Poladian, and F. Ouellette, Electron. Lett. **30**, 1620 (1994).
[4] M. Ibsen, B. J. Eggleton, M. G. Sceats, and F. Ouellette, Electron. Lett. **31**, 37 (1995).
[5] F. Ouellette, P. A. Krug, T. Stephens, G. Dhosi, and B. J. Eggleton, Electron. Lett. **31**, 899 (1995).
[6] H. Ishii, H. Tanobe, F. Kano, Y. Tohmori, Y. Kondo, and Y. Yoshikuni, IEEE J. Quantum Electron. **32**, 433 (1996).
[7] N. G. R. Broderick and C. M. de Sterke, Phys. Rev. E **55**, 3634 (1997).
[8] D. Marcuse, *Theory of Dielectric Optical Waveguides*, 2nd ed. (Academic, San Diego, 1991).
[9] G. W. Stroke, in *Optical Instruments*, edited by S. Flügge, Vol. XXIX Encyclopedia of Physics (Springer-Verlag, New York, 1967), Chap. 4.
[10] N. G. R. Broderick, C. Martijn de Sterke, and B. J. Eggleton, Phys. Rev. E **52**, 5788 (1995).
[11] B. J. Eggleton, C. M. de Sterke, and R. E. Slusher, Opt. Lett. **21**, 1223 (1996).
[12] J. E. Sipe, L. Poladian, and C. M. de Sterke, J. Opt. Soc. Am. A **11**, 1307 (1994).
[13] N. W. Ashcroft and N. D. Mermin, *Solid State Physics* (Saunders College, Philadelphia, 1976).
[14] C. M. de Sterke, D. G. Salinas, and J. E. Sipe, Phys. Rev. E **54**, 1969 (1996).
[15] L. Poladian, Phys. Rev. E **48**, 4758 (1993).
[16] E. Merzbacher, *Quantum Mechanics* (Wiley, New York, 1961).
[17] M. Born and E. Wolf, *Principles of Optics*, 6th ed. (Pergamon, Oxford, 1980).